XVI International Conference on Computational Plasticity. Fundamentals and Applications
COMPLAS 2021
E. Oñate, D. Peric, M. Chiumenti and Eduardo de Souza Neto (Eds)

FE-ANALYSIS OF END-NOTCHED BEAMS AND TENON JOINTS – *J*-INTEGRAL VERSUS COHESIVE ZONE MODELLING

TIMO CLAUS[*] AND WERNER SEIM[†]

[*] University of Kassel
Department of Building Rehabilitation and Timber Structures
Kurt-Wolters-Straße 3, 34125 Kassel, Germany
e-mail: claus@uni-kassel.de

[†] University of Kassel
Department of Building Rehabilitation and Timber Structures
Kurt-Wolters-Straße 3, 34125 Kassel, Germany
e-mail: wseim@uni-kassel.de

Key words: wooden connections, timber-to-timber joints, multiple tenon joints, fracture mechanics, Abaqus, *J*-integral, cohesive zones

Abstract. Improved wood-based materials, on the one hand, and computer-operated machinery, on the other, enable new types of timber-to-timber joints. Furthermore, new materials, such as laminated veneer lumber with cross-layers made of soft- or hardwood offer new possibilities regarding timber-to-timber connections like tenon and mortise. Experimental investigations have shown comparable failure mechanisms in mode I and mode II for tenon and multiple tenon joints, dovetail connections as well as for end-notched beams. In the field of fracture mechanics different concepts exists to describe the fracture behavior such as the strain energy release rate, the stress intensity factors and the *J*-integral method for timber-to-timber joints.
In this study the *J*-integral was determined around the crack tip in a finite element (FE) model in timber connections. The failure criterion was defined when the *J*-integral equals the energy release rate in mixed mode of the timber material. A sensitivity analysis showed that the failure load was not depending significantly on the initial crack length, the element size, the distance from the crack tip of the chosen contour and the size of the chosen contour.

In the next step, the model was validated on experimental test results of end-notched beams, tenon connections and multiple tenon connections. The experimental and numerical results showed very good accordance for different connection size and up to seven possible crack layers. Furthermore, a comparison between different fracture mechanic models with strain energy release rates and cohesive zones showed good performance of the new approach.

Afterwards, the FE model using the *J*-integral failure criterion was used to perform a comprehensive study of geometrical parameters for end-notched beams and tenon connections.

1 INTRODUCTION

In structural engineering finite element modelling with fracture mechanic analysis is a promising tool to predict the load bearing capacity of connections. Fracture analysis is necessary if connections are loaded in shear (mode I), tensions perpendicular to the grain (mode II) or rolling shear (mode III). The location of the possible crack layers and the direction of the crack growth should be known due to the anisotropy of the wood-based materials.
Different concepts of fracture mechanics were used in finite element modelling. On the one hand, cohesive zone modelling and *J*-integral analyses both use the specific fracture energy of the material G_c to predict critical crack growth. On the other hand, the concept of stress intensity factors uses the fracture toughness K_c of the material and probabilistic methods can be used to calculate the capacity considering specific stress criterions.

In this study the load bearing capacity of timber connections loaded in combinations of mode I and II such as end-notched beams and tenon joints will be investigated experimentally. Afterwards, the connections will be analysed with two different finite element models based on cohesive zones (1) and *J*-integral (2). Both structural models will be described for the use as engineering applications to predict maximum strength of this type of timber connections. Finally, a comprehensive parametric study will be performed to show the influence of the geometrical parameters in detail.

2 STRUCTURAL MODELS

2.1 Cohesive Zones

A numerical model was developed in a two-dimensional model within the framework of the commercial software package *ABAQUS* [1]. The failure areas were predefined at the lower edge of the notches. The material parameters of the cohesive elements are implemented according to *Claus and Seim* [2]:

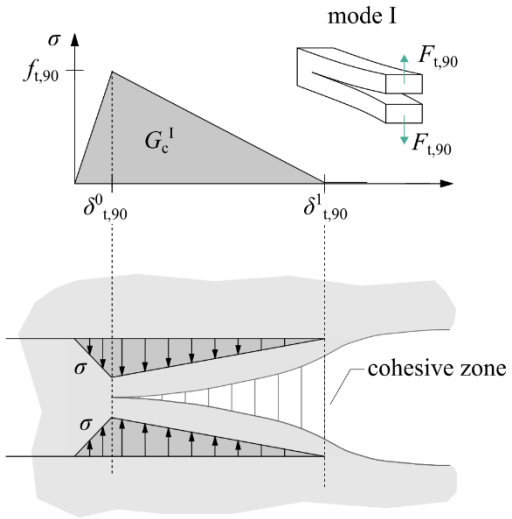

Figure 1: Example for crack growth under loading in mode I.

The characteristic of the elements is mainly classified in three phases. Initially, elastic behaviour is assumed until the stress failure criterion is reached. Subsequently, softening of the elements occurs until the fracture energy is completely dissipated. Finally, the cohesive elements have zero stiffness (Fig. 1). The traction separation law in ABAQUS is defined via "quads damage". Therefore, a stress-dependent failure criterion must be defined. Damage is assumed to initiate when the predefined failure criterion (Eq. (1)) reaches the value of one. The tension stresses perpendicular to the grain $\sigma_{t,90}$ and the shear stresses parallel τ are considered and compared to the corresponding strengths $f_{t.90}$ and f_v:

$$\left(\frac{\sigma_{t,90}}{f_{t,90}}\right)^2 + \left(\frac{\tau_v}{f_v}\right)^2 = 1 \tag{1}$$

An effective deformation δ_m is determined by the combination of deformation in each direction $\delta_{t,90}$ and δ_v:

$$\delta_m = \sqrt{\delta_{t,90}^2 + \delta_v^2} \tag{2}$$

The effective deformation is used to define the stiffness variable D with the maximum displacement δ_m^{max} and the displacement δ^0 and δ^1 at the beginning and at the end of the softening period. D is defined as

$$D = \frac{\delta_m^1(\delta_m^{max} - \delta_m^0)}{\delta_m^{max}(\delta_m^1 - \delta_m^0)}. \tag{3}$$

The starting value of D is zero and increases to a maximum of one when the energy is dissipated. The stiffness variable influences the stresses within the cohesive elements. Tensile stresses in mode I show softening behaviour, whereas compressive stresses are not influenced by the stiffness variable:

$$\text{Modus 1: } \sigma = \begin{cases} (1-D)\bar{\sigma} & \text{für } \sigma \geq 0 \\ \bar{\sigma} & \text{für } \sigma < 0 \end{cases} \tag{4}$$

$$\text{Modus 2: } \tau = (1-D)\bar{\tau} \quad \text{für } \sigma \geq 0 \text{ und } \sigma < 0 \tag{5}$$

The stress components σ and τ are the values predicted by the elastic traction-separation behaviour for the current strains. The shear stresses in mode II at maximum deformation are zero and are not affected by alternating directions. Damage evolution is defined as linear. Thus, the displacements at complete softening are derived by the total fracture energy G_c of each mode:

$$G^I = \frac{1}{2}\sigma\delta_{t,90}^1 \qquad \text{and} \qquad G^{II} = \frac{1}{2}\tau\delta_v^1 \tag{6}$$

To compare the different models ist is necessary to use the multimode fracture energy in mode I and II. G^{I+II} is the sum of the fracture energy in each mode:

$$G^{\mathrm{I+II}} = G^{\mathrm{I}} + G^{\mathrm{II}} \tag{7}$$

The fracture energy $G_c^{\mathrm{I+II}}$ equals the geometrical area under the tension separation law (Fig. 1). The failure criterion for multimode fracture is then defined as

$$\frac{G^{\mathrm{I+II}}}{G_c^{\mathrm{I+II}}} = 1 \quad . \tag{8}$$

A FE model with four cohesive layers is shown in Figure (2). The model consists of CPS4R quadratic elements. The mesh was 5.0 mm to ensure numerical convergence. Two-dimensional element types COH2D4 with four nodes were chosen with an element thickness of 0.01 mm to represent brittle tension failure. The specified damping factor for numerical stabilization was chosen to 0.0002.
A deformation w was applied via a reference point (RP) in the middle of the beam on a load distribution plate. Symmetry was used to reduce calculation time. The length of the beam was then around $2h$. Under the tenons the soft support of the main beam was considered via contact to a second reference point which was represented by a compliance k_s. The stiffness of the experimental test series was reproduced accurately. The support load for this model was given from the reference point and is called V_{coh}.
Two different timber materials were used in the models. Solid wood with the strength class C24 according to EN 338 [3] and glued laminated timber GL24h according to EN 14080 [4] were implemented with mean values of stiffness and fracture parameters (Table 1). A documentation of the determination of the mean values of the strength parameters in mode I and II was performed in *Claus* [5]. The multimode fracture energy $G_c^{\mathrm{I+II}}$ was determined from experimental and numerical investigations by *Franke* [6] and already discussed by *Jockwer* [7].

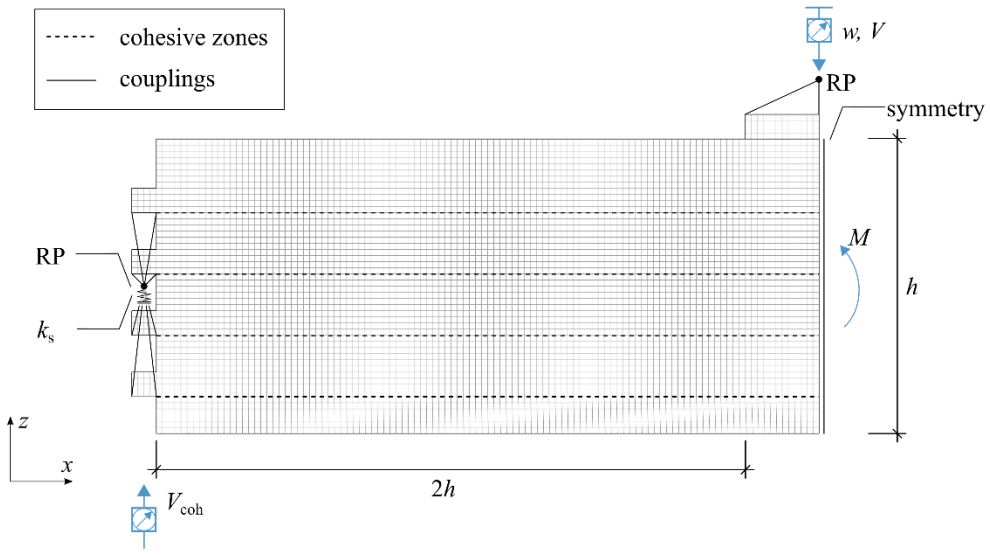

Figure 2: FE-model of test specimen TS4 with four cohesive layers.

Table 1: Mean values of material stiffness and fracture parameters.

	E_x N/mm²	E_z N/mm²	G_{xz} N/mm²	ν_{xz} -	ν_{yz} -	$f_{t,90}$ N/mm²	f_v N/mm²	G_c^{I+II} N/mm
C24	11000	370	690	0.45	0.24	0.7	5.6	0.21
GL24h	11500	300	650	0.45	0.24	0.7	4.4	0.21

2.2 *J*-Integral

Another parameter to describe the fracture behaviour of solids in the framework of linear elastic fracture analysis is the *J*-integral. The *J*-integral is a path integral on the contour Γ around the crack tip and was nearly discovered simultaneously by *Rice* [8] and *Cherepanov* [9].

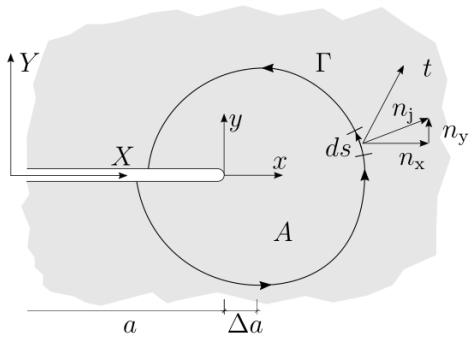

Figure 3: *J*-Integral at the crack tip from *Kuna* [10].

Because of the path independency, only a subsystem around the crack tip needs to be investigated (Figure 3). The path encloses the area *A*. The potential of the inner energy can be expressed by the deformation energy density *U*. For an elastic material is *U* the deformation energy per volume.

$$U = \frac{1}{2}\left(\sigma_x \frac{\partial u}{\partial x} + \tau_{xy}\left(\frac{\partial u}{\partial y} + \frac{\partial v}{\partial x}\right) + \sigma_y \frac{\partial v}{\partial y}\right) \tag{9}$$

The stress tensor t_i includes the stresses σ_{ij} acting from outside the area *A*. The vector n_j is orthogonal to the contour Γ.

$$t_i = \sigma_{ij} n_j \tag{10}$$

If no other external forces act on the subsystem and no damages or cracks occur in the enclosed area, the conservation of energy can be expressed with the path integral:

$$\int_\Gamma \left[U dy - t_i \frac{\partial u_i}{\partial x} ds\right] = 0 \tag{11}$$

The length d*s* discribes a segment on the contour Γ. Under crack progress in local *X*-direction the area *A* moves from a to $a + \Delta a$. The change of potential energy dΠ under crack progress Δa can be expressed compareable to the energy release rate *G* with the *J*-Integral. For a contour enclosing a crack the following expression from *Kuna* [10] can be used:

$$G = -\frac{d\Pi}{da} = J \equiv \int_{\Gamma} \left[U dy - t_i \frac{\partial u_i}{\partial x} ds \right] \tag{12}$$

The critical crack progress starts when J reach the value J_c. The fracture criteria is

$$J = J_c \leq G_c. \tag{13}$$

To be able to compare the multi-mode critical energy release rate G_c^{I+II} it needs to be shown that:

$$J = J^{I+II} = J^{I} + J^{II}. \tag{14}$$

It was proofed that the J-integral is path independent. Thus, every path including a crack tip can be used for the determination of J. A simple comparison with the calculation of the energy release rate G was performed for the double cantilever beam in *Claus* [5]. The J-integral was already used from other authors for example to determine stress intensity factors in FE Models of bolted connections by *Borth* [11].
In the finite element model, the contours were defined automatically around the crack tip (Figure 4a). Only quadratic elements were used for the determination of J in *ABAQUS* [1].
The support load V was determined depending on the J-integral (Figure 4b). Then, the critical support load V_c was evaluated for the critical energy release rate G_c^{I+II}.
To check the influence of model parameters, the initial crack length a, the element size a_E and the distance of the contour from the crack tip r_i were investigated. Only minor deviations of the critical support loads were observed. The initial crack length was then fixed to a = 40 mm because of little increase of J for very small values and the element size was set to a_E = 5 mm for the model an reduced to a = 1 mm in the area of the evaluated contours. For the following calculations the contour integral Γ_1 will be evaluated.
The calculation of the J-integral reacts more or less insensitive under changing the stiffness parallel to the grain E_x and the fracture parameter G_c^{I+II} of the models.

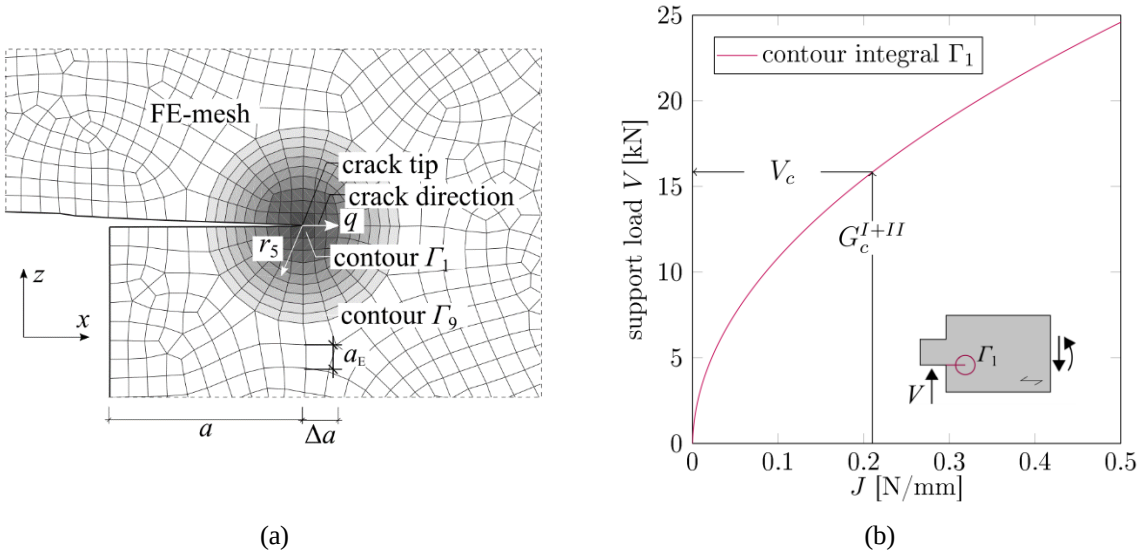

(a) (b)

Figure 4: (a) FE-model with the implementation of contours around the crack tip and (b) support load V depending on the J-integral for the contour Γ_1.

3 EXPERIMENTAL INVESTIGATIONS ON TENON JOINTS

All in all, n = 33 experimental tests on tenon and multiple tenon joints were performed (see *Claus and Seim* [2] and *Claus* [5]). A deformation $w_{2,o}$ was applied at the middle of the secondary beam and the support load V was calculated for the joint between the main beam and secondary beam (Figure 5a). Connections with one, two, four and seven tenons were carved out at the main beam on a joinery machine. Two different beam sizes and materials were used (Table 2). The distance between the applied load and the tenon joints was always $2h$.

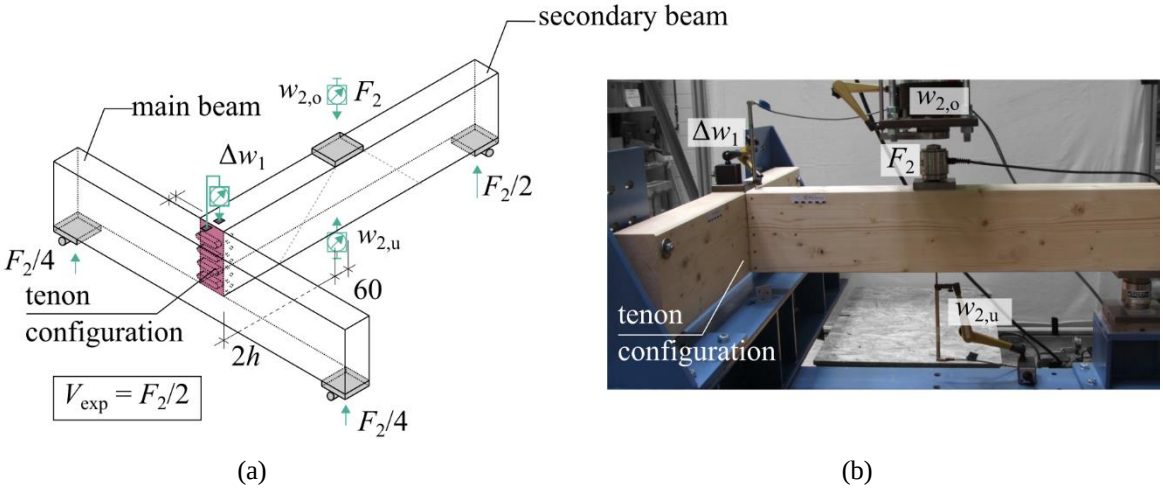

(a) (b)

Figure 5: Tenon and multiple tenons joints (a) schematic test set-up and (b) photo of the test set-up.

During the tests, the deformation w_1, w_2 and the applied load F_2 was recorded. Until failure all specimens showed a linear elastic deformation behaviour until sudden failure occured due to crack propagation along the wooden fibre under the tenons. The location of the cracks was depending on the number and location of the tenons. The mean values of the failure load $\bar{V}_{exp,max}$ increased with the number of tenons n_t in the connections and the size of the beams. The coefficient of variation (COV) is highly depending on the material as well as the number of tenons. The more tenons the less is the variation of test results within one test configuration.

Table 2: Geometrical parameters and experimental resistance of tenon joints.

	n_t	material	b	h	n	$\bar{V}_{exp,max}$	COV
	-	-	mm	mm	-	kN	%
TS1	1	C24	100	240	5	13.8	20
TS2	2	C24	100	240	6	17.4	30
TS4	4	GL24h	100	240	5	37.4	6
TM2	2	GL24h	160	380	6	52.1	13
TM4	4	GL24h	160	380	6	69.4	11
TM7	7	GL24h	160	380	5	78.1	5

4 VALIDATION AND COMPARISON

In the next step, the numerical results of the cohesive zone model and the *J*-integral model will be compared to the experimental failure loads of the tenon and multiple tenons joints.
Figure 6a shows the single test results $V_{exp,max}$ of each test configuration on the numerical failure load of the cohesive zone model $V_{c,coh}$. Most of the test configuration are well reproduced from the cohesive zone model. Thus, the value G_c^{I+II} = 0.21 N/mm for multimode failure of notches seems to be a good assumption. Test series TS1 and TS2 (solid timber) are overestimated from the model and series TM7 is slightly underestimated by the simulation. Modelling with cohesive zones allows to consider on the one hand the reinforcements of cracks and on the other side the detailed load deformation behaviour can be compared to the experimental data (comp. *Claus and Seim* [2]).

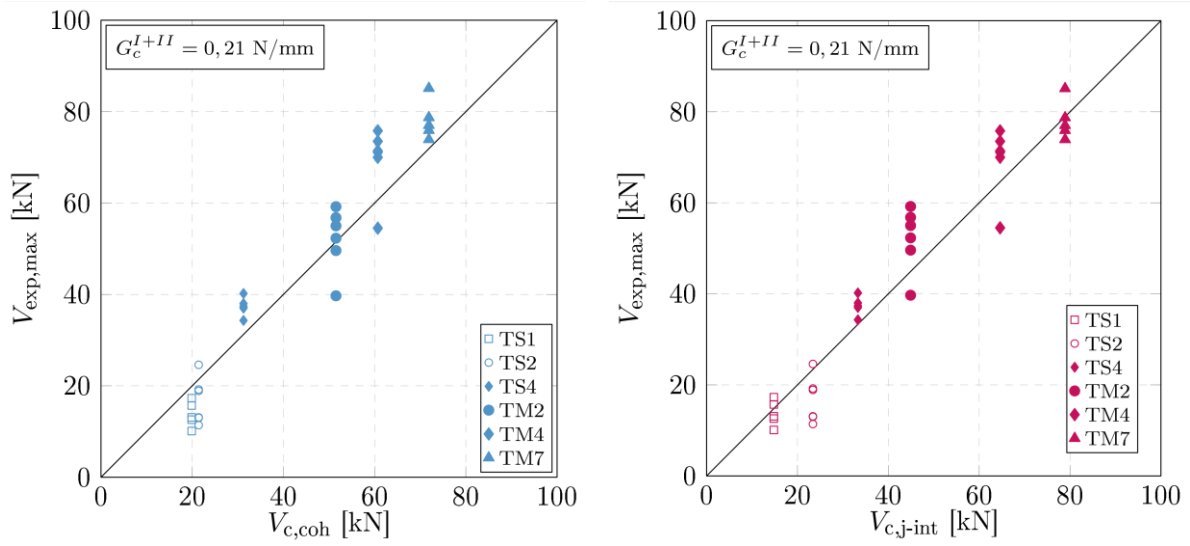

Figure 6: Comparison of the experimental test results with (a) the results from the cohesive zone model and (b) the results from the *J*-integral model.

The experimental failure loads compared to the failure loads from the *J*-integral model are shown in Figure 6b. For all series, the failure load of the model is in the variety of the experimental test results. Especially the Series TS1 with only one tenon made of solid timber TS1 and with seven tenons made of glulam TM7 are well reproduced by the *J*-integral model. Thus, just like for the cohesive zone model the specific fracture energy G_c^{I+II} seems to be a good approach also for the *J*-integral model.
On the one hand, one disadvantage of the *J*-integral model is that no reinforcements could be modelled in the crack area because the crack surfaced need to be stress-free. On the other hand, it is a pure linear elastic model and therefore the computing time is reduced to a few seconds for each model. Combined with a parametric model, the *J*-integral could be used for comprehensive studies of geometrical and materials parameters. An example for a parametric study of geometric parameters was performed for end-notched beams and single tenon joints.

5 STUDY OF GEOMETRICAL PARAMETERS

5.1 End-notched Beams

In this part, two decisive parameters of end-notched beams were studied. First the beam height h and secondly the notch ratio αh was varied. The beam width was b = 200 mm and the notch length ratio was $\beta = 0.1h$. The initial crack length was chosen constantly to a = 40 mm. The material was GL24h with parameters chosen according to Table 1. All in all 55 different models were built.

Figure 7a shows the variation of the height h in nine steps between 100 mm and 1500 mm. Additionally the notch ratio was varied between α = 0.50 and 0.95. The fracture load increases rapidly for small beam heights. No asymptotic course is visible, thus with higher beam size the failure loads will always increase.

The notch ratio α was varied in six steps in Figure 7b. The failure load $V_{c,int}$ increases over proportional with higher values of α. Thus, the location of the potential crack layer has a significant influence of the load bearing capacity of end-notched beams.

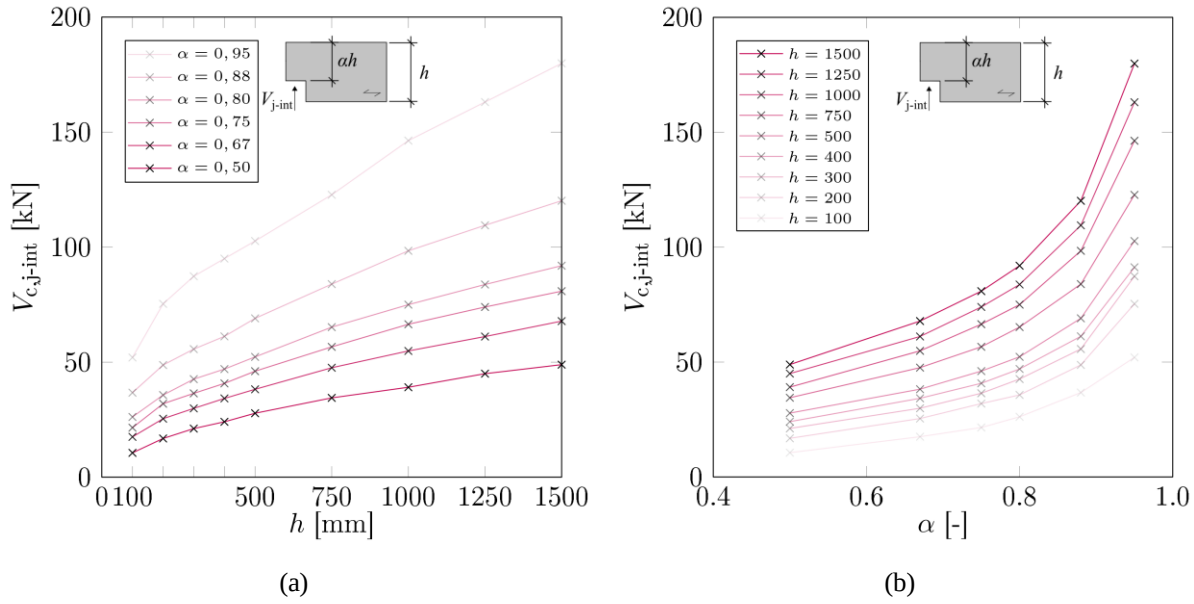

(a) (b)

Figure 7: Variation of (a) the height h of the beam and (b) the height of the notch αh.

5.1 Tenon joints

A second parametric analysis was performed for single tenon joints. In this case, the cross section of the beam was fixed to b = 100 mm and h = 240 mm according to the geometry of test series TS1. The elastic material parameters were chosen to GL24h according to Table 1. The distance from the support to the notched corner was set to $\beta = 0.1h$ and the initial crack length was again a = 40 mm. In this study, the position of the tenon (e.g. the crack layer) was varied with the parameter α and on the other hand the tenon height h_t was varied with the parameter $\gamma = h_t/\alpha h$.

Figure 8a shows, comparable to Figure 7b the influence of the notched ratio α of the tenon connection. The failure load $V_{c,j\text{-}int}$ increases with higher notch ratios. Consequently, the highest capacity will be reached when the crack layer is arranged near to the bottom side of the beam.
In Figure 8b the failure load $V_{c,j\text{-}int}$ is shown depending on the tenon high $\alpha\gamma h$ for different positions of the crack layer. When the crack layer supposed to be in the middle of the beam ($\alpha = 0.50$), the tenon high has minor influence on the failure load of the tenon connection. For tenons arranged more on the bottom side of the beam, the failure load increases with increasing tenon height. Especially for notch ratios of $\alpha > 0.67$, the failure loads did not increase for tenon heigh ratio of $\gamma \geq 0.70$. These results visualized that there is an optimum of tenon height when $\gamma = 0.70$. These findings could be used to optimize the single and multiple tenons connections in future research.

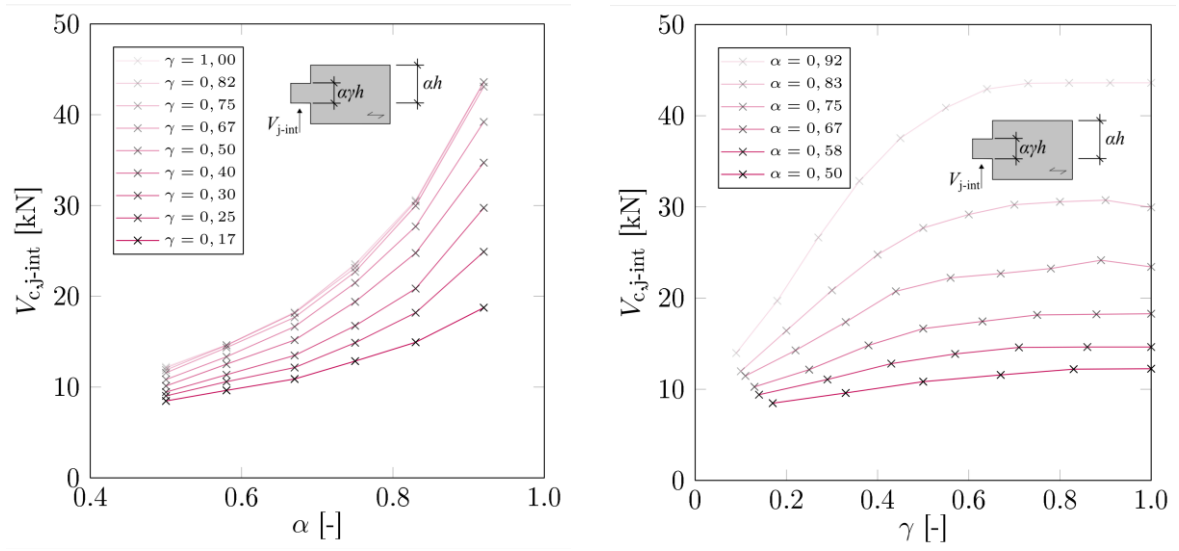

Figure 7: Variation of (a) the position of the crack layer with αh and (b) the height of the tenon $\alpha\gamma h$.

6 SUMMARY AND CONCLUSION

In this conference proceeding two finite element models were presented to determine the failure loads of notched timber beams. Both models, the cohesive zone model (1) and the J-integral model (2) showed good accordance to the experimental results regarding multimode failure in mode I and II.
The advantage of the cohesive zone method is, that it provides detailed information of the load deformation behaviour of the entire timber parts. Furthermore, the implementation of reinforcements of the possible crack layers is possible. The disadvantage of the cohesive zone model is the computing time. The non-linear behaviour of the cohesive elements requires proper settings to reach numerical convergence.
A parametrically build up model of a pre-cracked structure and pre-defined contours around the crack tip allows proper results with the *J*-integral model. To evaluate failure loads from this

model only linear elastic element behaviour is needed. This saves computing time in particular for comprehensive studies of geometrical parameters and material properties.
Finally, the study of geometrical parameters of end-notched beams and tenon joints illustrated the reliability and the scope of possibilities for this innovative finite element analysis. The method showed new results of the geometrical influence of tenon connections – with only little effort.
For the future the application of the *J*-integral model and the influence of the initial crack length should be checked for timber structures loaded in mode II only.

REFERENCES

[1] Abaqus 6.12-3. *Abaqus 6.12-3 - Dassault Systèmes Simulia Corporation*. Dassault Systèmes Simulia Corporation (2012).

[2] Claus, T. and Seim, W. Development of the multiple tenon timber connection based on experimental studies and FE simulation. *Engineering Structures* (2018) 173:331-339. doi: 10.1016/j.engstruct.2018.06.102

[3] EN 338. *Structural timber - Strength classes*; German version EN 338:2016 (2016).

[4] EN14080. *Timber structures - Glued laminated timber and glued solid timber - Requirements*; German version EN 14080:2013 (2013).

[5] Claus, T. *Design and calculation of end-notched beams and tenon joints in timber constructions* (in German: Entwurf und Berechnung von ausgeklinkten Trägerauflagern und Zapfenverbindungen im Holzbau). PhD-Thesis, University of Kassel, Germany, (2020). doi:10.17170/kobra-202009281850

[6] Franke, B. *To assess the load-bearing capacity of beam notches in coniferous timber* (in German: Zur Bewertung der Tragfähigkeit von Trägerausklinkungen in Nadelholz). PhD-Thesis. Bauhaus Universität Weimar, Germany, (2008).

[7] Jockwer, R. *Structural behaviour of glued laminated timber beams with unreinforced and reinforced notches*. Phd-Thesis. ETH Zürich, Switzerland, (2015).

[8] Rice, J.R. A Path Independent Integral and the Approximate Analysis of Strain Concentration by Notches and Cracks. *Journal of Applied Mechanics* (1968) 35:379-386.

[9] Cherepanov, G.P. The Propagation of Cracks in a Continuous Medium. *Journal of Applied Mathematics and Mechanics* (1967) 31:503-512.

[10] Kuna, M. *Finite elements in fracture mechanics: theory - numerics - applications*. Springer, (2013).

[11] Borth, O. Schober, K.-U. Rautenstrauch, K. *Load-Carrying Capacity of Perpendicular to the Grain Loaded Timber Joints with Multiple Fasteners*. Proceeding of CIB W18 Meeting, 35-7-8, Kyoto, Japan, (2002).